Journal of Power Sources 184 (2008) 604–609

Contents lists available at ScienceDirect

Journal of Power Sources

journal homepage: www.elsevier.com/locate/jpowsour

Sol–gel synthesis of $Mg_{1.03}Mn_{0.97}SiO_4$ and its electrochemical intercalation behavior

Zhenzhen Feng, Jun Yang*, Yanna NuLi, Jiulin Wang

Department of Chemical Engineering, Shanghai Jiao Tong University, Shanghai 200240, PR China

ARTICLE INFO

Article history:
Received 4 January 2008
Received in revised form 6 May 2008
Accepted 8 May 2008
Available online 16 May 2008

Keywords:
Magnesium manganese silicate
Sol–gel
Intercalation
Cathode material
Rechargeable magnesium batteries

ABSTRACT

Magnesium manganese silicate ($Mg_{1.03}Mn_{0.97}SiO_4$) was prepared by a sol–gel method and evaluated as an intercalation electrode material for rechargeable magnesium batteries. The crystalline $Mg_{1.03}Mn_{0.97}SiO_4$ phase was obtained after heating at 900 °C and its electrochemical performance was characterized at room temperature. The pure magnesium manganese silicate exhibits a relatively low reversible specific capacity in the electrolyte comprising 0.25 mol L^{-1} $Mg(AlCl_2EtBu)_2$/THF owing to its poor electronic conductivity. Using a ball mill in the presence of acetylene black, and in situ carbon coating, the resulting composites present an improved discharge voltage plateau (1.6 V *vs.* Mg/Mg^{2+}) and increased discharge specific capacity (92.9 mAh g^{-1} at a C/50 rate). The Mg lower price and its feasibility for rechargeable batteries make magnesium manganese silicate an attractive candidate for rechargeable magnesium based batteries.

1. Introduction

In recent years, considerable research interest has focused on rechargeable magnesium batteries because of the great advantages of metallic magnesium in low price, large theoretical specific capacity, very low potential *vs.* NHE and high safety [1]. In 2000, Aurbach et al. developed some new electrolyte solutions based on ethers and magnesium aluminates, in which 0.25 mol L^{-1} $Mg(AlCl_2BuEt)_2$/THF shows the best performance [2]. This achievement boosts the development of rechargeable magnesium batteries to a new level. However, the choice of cathode materials is limited due to the difficulty in achieving reversible magnesium intercalation/de-intercalation processes in many hosts owing to the strong polarization of small and divalent Mg^{2+} ion. So far, $Mg_xMo_3S_4$ ($0 < x < 1$), whose maximum specific charge is 122 mAh g^{-1}, can be regarded as the most effective magnesium intercalation electrode material [2]. The other relevant reports mostly focused on different transition metal sulfides or oxides, which presented either a small discharge capacity or a low discharge voltage [3–7]. Therefore, search for new types of competitive cathode materials is necessary for the development of rechargeable magnesium batteries.

Li_2MSiO_4 (M represents certain transition metal elements) have been recently reported as new cathode materials for rechargeable lithium batteries, and it is possible to exchange two electrons per transition metal atom without any significant changes in the crystal structure [8–11]. The lattice stabilization effect deriving from the strong covalent Si–O bond could translate into electrochemical and chemical safety in a voltage domain. In addition, the transition metal M should possess more than two neighboring oxidation states to achieve the ultimate goal to exchange both lithium ions. Among the transition metal silicates, Li_2MnSiO_4 is a good choice for potential cathode material [12–17]. On the other hand, it was reported that the strong inductive effect of the polyanion can moderate the transition metal redox couple to generate a relatively high operating voltage [18]. Enlightened by the existing results and considerations related to Li_2MnSiO_4, we attempted to investigate the manganese silicate compound as magnesium intercalation electrode.

In view of that the theoretical capacity of $Mg_{1.03}Mn_{0.97}SiO_4$ can reach as high as 314 mAh g^{-1} based on the assumption of full charge of one Mg, we have prepared its nanosized powder sample by a sol–gel route and investigated its electrochemical intercalation behavior in the present work.

2. Experimental

2.1. Preparation and characterization of $Mg_{1.03}Mn_{0.97}SiO_4$

$Mg_{1.03}Mn_{0.97}SiO_4$ was prepared by a sol–gel process. The starting precursors were magnesium acetate tetrahydrate ($MgAc_2{\cdot}4H_2O$), manganese(II) acetate tetrahydrate ($MnAc_2{\cdot}4H_2O$), and tetraethyl silicate ($C_8H_{20}O_4Si$). First, 0.02575 mol $MgAc_2{\cdot}4H_2O$

* Corresponding author. Tel.: +86 21 54747667.
E-mail address: yangj723@sjtu.edu.cn (J. Yang).

0378-7753/$ – see front matter © 2008 Elsevier B.V. All rights reserved.
doi:10.1016/j.jpowsour.2008.05.021

and 0.02425 mol $MnAc_2{\cdot}4H_2O$ were added into 60 mL ethanol under electromagnetic stirring. Second, 0.025 mol tetraethyl silicate with molar ratio of 1.03:0.97:1 for Mg, Mn and Si was added to the obtained solution and kept thoroughly stirring. Next, the obtained mixture was further stirred at 60 °C for at least 24 h under argon atmosphere to form a white thick liquid, which was then dried at 100 °C under vacuum overnight to give a white powder. After thoroughly grinding with a mortar and pestle, the obtained powder was heated in a pure argon atmosphere at 500 °C for 5 h, followed by final firing at various temperatures for 24 h in a conventional tube furnace under argon atmosphere.

In order to increase the electronic conductivity, reduce or hinder particle agglomeration, thus improve the electrochemical performance of the sample, two kinds of carbon coating methods were adopted: (i) mechanical coating by ball milling, (ii) in situ pyrolysis of carbon precursor. For mechanical carbon coating, the resulted $Mg_{1.03}Mn_{0.97}SiO_4$ was ball-milled with 20 wt.% acetylene black for 4 h to obtain $Mg_{1.03}Mn_{0.97}SiO_4$/AB composite. The alternative method, designated as in situ carbon coating, was to add sucrose during the hydrolysis process, followed by drying and heat treatment. The resulting product is named as $Mg_{1.03}Mn_{0.97}SiO_4$/C.

The X-ray powder diffraction pattern was recorded on a D/MAX-2200/PC Rigaku diffractometer equipped with Cu Kα radiation (λ = 0.15406 nm) at a rate of 4° min^{-1}. The 2θ range used in the measurement was from 15° to 75°. The particle morphology was observed using scanning electron microscopy (SEM) on a JEOL field-emission microscope (JSM-7401F) and transmission electron microscopy (TEM) on a JEOL high-resolution electron microscope (JEM-2010). The coated carbon was detected by energy dispersive spectrometer (EDS) and the carbon content in the composite material was determined by the carbon elemental analysis combustion method on a CHNS/O elemental analyzer (American PerkinElmer).

2.2. Electrochemical measurements

The electrodes were prepared by casting and pressing a 78:12:10 weight–ratio mixture of as-synthesized $Mg_{1.03}Mn_{0.97}SiO_4$ (or its composites with carbon), acetylene black and polyvinylidene fluoride (PVDF) binder onto a copper foil current collector followed by drying in vacuum at 120 °C for 8 h. Test cells were assembled in a glove box under pure argon atmosphere (less than 1 ppm of water and oxygen). Electrochemical magnesium intercalation was evaluated via CR2016 coin-type cells containing 0.25 mol L^{-1} $Mg(AlCl_2BuEt)_2$/THF with magnesium strip counter electrode and Entek PE membrane separator. Charge–discharge measurements of the coin-type cells were carried out at various rates on a Land battery measurement system. The voltage was kept below 2.1 V (*vs.* Mg/Mg^{2+}) to avoid degradation of the electrolyte and corrosion of the copper current collector. There are 30 s rest between both charge and discharge voltages. Cyclic voltammograms (CVs) and AC impedance spectroscopy were measured in three-electrode cells inside the glove box at room temperature using CHI650C Electrochemical Workstation (Shanghai, China). The impedance measurements were carried out by applying 5 mV amplitude over a frequency range of 100.00 kHz to 0.1 Hz.

3. Results and discussion

X-ray diffraction (XRD) was used to determine the crystallinity and phase structure of the synthesized materials. Fig. 1 shows the XRD patterns of $Mg_{1.03}Mn_{0.97}SiO_4$ that were heat-treated at various temperatures under pure argon atmosphere. The material, resulting from the sol–gel reaction and drying overnight at 100 °C under vacuum, shows various weak XRD peaks, corresponding to a low-

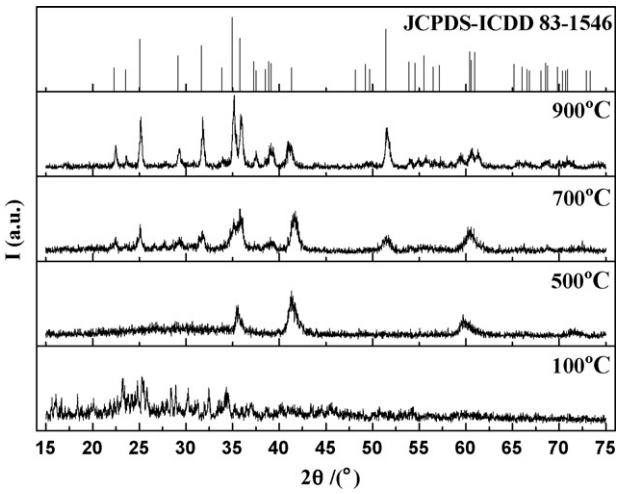

Fig. 1. XRD patterns of $Mg_{1.03}Mn_{0.97}SiO_4$ obtained at various treatment temperatures, and its standard pattern (JCPDS-ICDD 83-1546).

crystalline and multi-component character. By heat treatment at 500 °C, the crystallized product begins to form. After further firing at 700 °C, all the characteristic peaks appear. The difference in XRD responses between the samples calcinated at 700 and 900 °C suggests that complete crystal growth of $Mg_{1.03}Mn_{0.97}SiO_4$ can be realized at relatively high temperature. The diffraction peaks of the sample after calcination at 900 °C are fully consistent to the standard structure indexed by JCPDS-ICDC 83-1546. Unreacted starting materials and metallic oxide phases cannot be detected in the product.

The crystal system of $Mg_{1.03}Mn_{0.97}SiO_4$ belongs to orthorhombic, and the refined cell parameters are: $a = 4.794$, $b = 10.491$ and $c = 6.123$ Å; space group: Pbnm (62). The refined crystal structure in polyhedral representation with the co-ordinate system is presented in Fig. 2a. Typical octahedral and tetrahedral patterns can be recognized. Alternate sites of Mg1Mn1 (represents as balls with 1) and Mg2Mn2 (represents as balls with 2) are within the octahedra and Si sites are within the tetrahedra, while oxygen atoms are in the corners. Fig. 2b shows the corresponding ball–stick model and the relevant atomic parameters are given in Table 1. The obtained crystal structure reveals mixed site occupation of the same octahedral sites by Mg and Mn, but with different atomic site occupied fraction (S.O.F., see Table 1). That is to say, there are two kinds of possible positions for Mg atoms in this structure with different geometrical circumstances.

The sol–gel synthesis technique offers a convenient way for producing powder materials with small particle size by homogeneous mixing of reagents on an atomic scale. It is well known that nanosized materials may have better electrochemical performance than bulk ones. A decrease in the average particle size means a shorter diffusion length for magnesium ions in the host and higher surface area in contact with the electrolyte solution, which may improve

Table 1
Atomic parameters of $Mg_{1.03}Mn_{0.97}SiO_4$

Atom	S.O.F.	*x*/*a*	*y*/*b*	*z*/*c*
Mn1	0.08	0	0	0
Mg1	0.92	0	0	0
Mn2	0.89	0.9870	0.2790	0.2500
Mg2	0.11	0.9870	0.2790	0.2500
Si1		0.4226	0.0910	0.2500
O1		0.7585	0.0867	0.2500
O2		0.2301	0.4489	0.2500
O3		0.2782	0.1590	0.0374

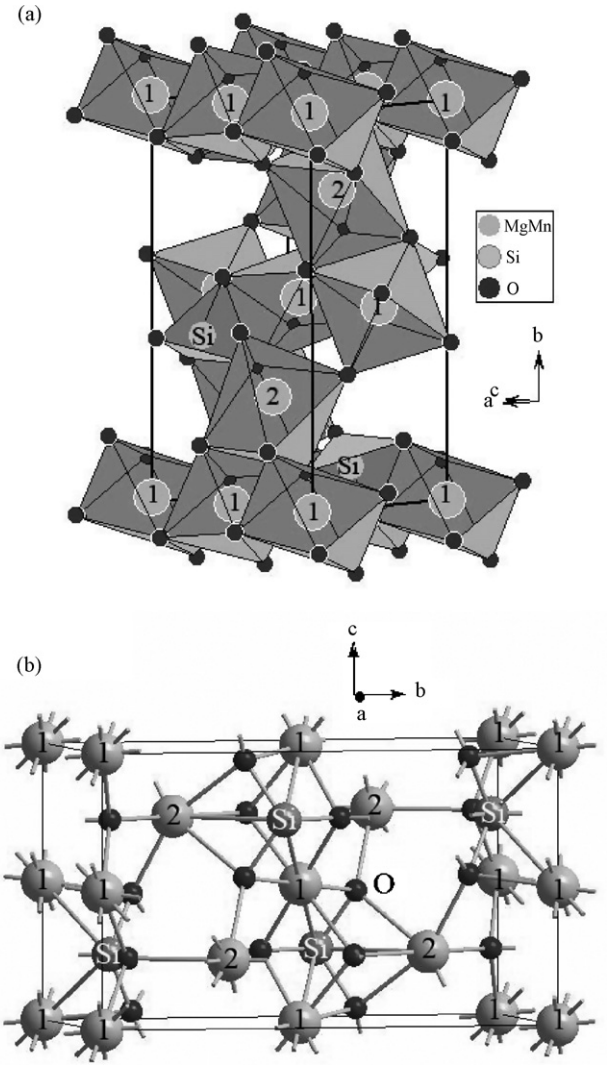

Fig. 2. Ordered crystal structure of $Mg_{1.03}Mn_{0.97}SiO_4$. Alternate Mg1Mn1 and Mg2Mn2 are shown as balls marked with 1 and 2, respectively. Unit cell and cell axes are outlined. (a) Depiction of polyhedral connectivity; (b) ball–stick model.

the intercalation kinetics. Fig. 3 exhibits the morphology of the obtained $Mg_{1.03}Mn_{0.97}SiO_4$ particles without (Fig. 3a) and with in situ carbon coating (Fig. 3b). The pure product presents a relatively wide particle size distribution from tens of nanometers (first distribution) to several microns because of the particles' aggregation (Fig. 3a). In order to suppress the agglomeration and enhance the powder's electronic conductivity, the fired material prepared at 900 °C was mechanically ball-milled in the presence of acetylene black. After such a treatment, the agglomerated extent is decreased and the electrochemical performance is improved obviously (see Fig. 5a). On the other hand, the homogeneous particle dispersion is obtained by in situ carbon coating and the particle size is reduced to less than one hundred nanometer (see Fig. 3b). The TEM imaging further shows that the primary particle size is about 30–80 nm and the outer grey layer on the $Mg_{1.03}Mn_{0.97}SiO_4$ particle is estimated to be less than 10 nm (see Fig. 4a), which was affirmed to be carbon by EDS analysis. In fact, the solution phase mixing process can ensure uniform sucrose dispersion in the gel product. During the subsequent high-temperature treatment, sucrose will go through a melting state, which is favor of its homogeneous coating and thus suppresses the particle agglomeration. The measurement result using the PerkinElmer 2400 Series II CHNS/O elemental analyzer indicates that the amount of carbon in the sample prepared by in situ carbon coating process was 9.76 wt.%. But as determined by TEM, not all the carbon was coated on the $Mg_{1.03}Mn_{0.97}SiO_4$ particles; part of it is embedded in the composite matrix (see Fig. 4b), which may also contribute to the improvement of the material's conductivity. In this article, we chose sucrose as the carbon precursor to improve the sample's electrochemical performance by increasing the electronic conductivity and reducing or hindering particle agglomeration. This technology has been used for improving the electrochemical performance of electrode materials and the feasibility has been verified by the experimental results [19,20]. It was reported that such carbon was disordered (hard carbon) and contained a large fraction of single grapheme layers [21]. In addition, the stacking of the single grapheme layers could be visualized as a "house of cards" that gave rise to nanoporosity in the materials. According to our experiment results, this type of carbon does not hinder the transfer of the Mg ions.

The charge–discharge measurements were carried out on the Land battery measurement system at room temperature. The electrochemical activities of the three silicate samples are inferred from Fig. 5a. When discharged at a C/25 rate, the specific capacity of $Mg_{1.03}Mn_{0.97}SiO_4$ was only 19.3 mAh g^{-1} and the discharge voltage plateau was very low and unobvious. This is the result of low intrinsic electronic conductivity and the slow magnesium diffusion

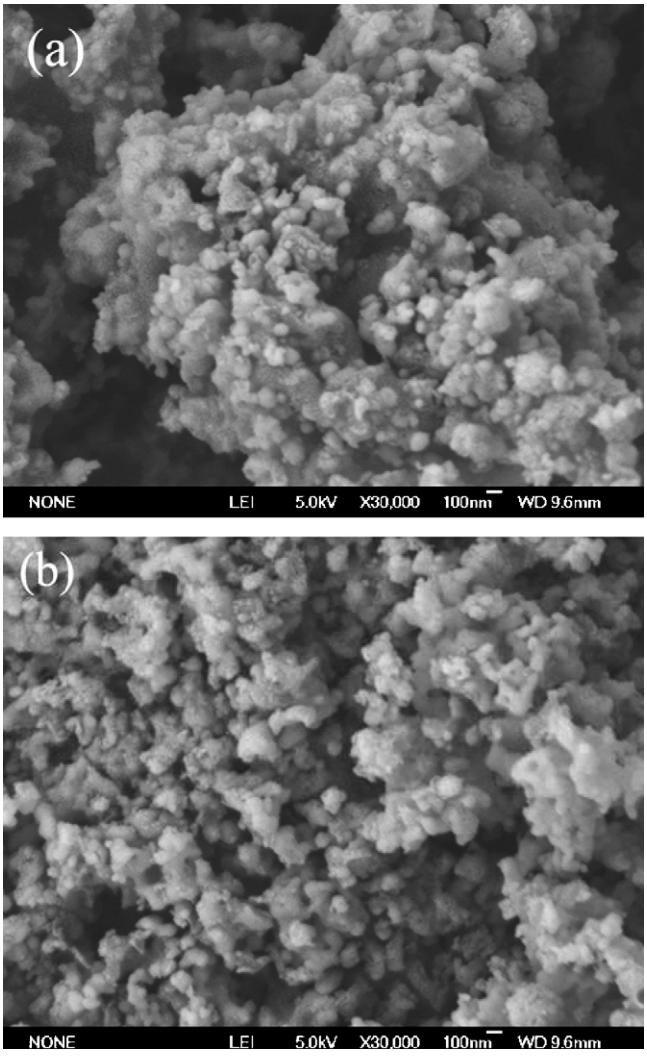

Fig. 3. SEM images of the $Mg_{1.03}Mn_{0.97}SiO_4$ (a), and $Mg_{1.03}Mn_{0.97}SiO_4$/C (b).

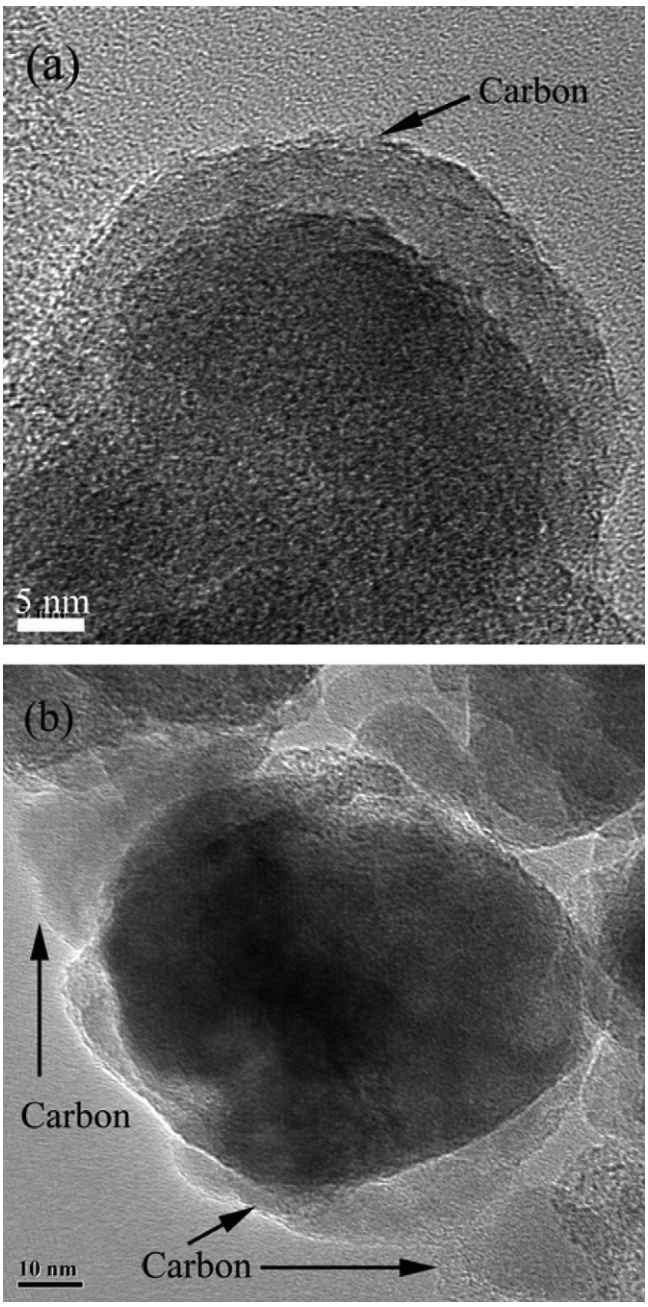

Fig. 4. TEM image of the $Mg_{1.03}Mn_{0.97}SiO_4$/C prepared by in situ carbon coating process.

kinetics within the grains of pure silicate. By simple ball milling with 20 wt.% acetylene black, the discharge specific capacity can be enhanced to 53.3 mAh g^{-1}. The best performance is obtained when in situ carbon coating is adopted. In situ carbon coating enhances the electronic conductivity greatly and also suppresses the agglomeration of nanoparticles. Thus, the electrochemical polarization is minimized due to the shortened ionic diffusion length within the particles and increased contacting area between reactant phase and electrolyte. As a result, the utilization of the active material is enhanced. The $Mg_{1.03}Mn_{0.97}SiO_4$/C composite gives the highest discharge capacity of 77.9 mAh g^{-1} at a C/25 rate, along with an enhanced and more flat discharge voltage plateau (mainly at 1.6 V *vs*. Mg^{2+}/Mg).

The electrochemical kinetic behavior of the $Mg_{1.03}Mn_{0.97}SiO_4$/C composite was further examined. Fig. 5b shows the intercalation curves at C/50, C/20 and C/10 rates for $Mg_{1.03}Mn_{0.97}SiO_4$/C. Accordingly, the specific intercalation capacities of 92.9, 63.6 and 36.8 mAh g^{-1} are obtained. The major intercalation voltage plateau is very flat and as high as about 1.6 V *vs*. Mg/Mg^{2+}. To the best of our knowledge, the discharge voltage plateau of 1.6 V *vs*. Mg/Mg^{2+} is the highest value among all of the reported cathode materials for rechargeable magnesium batteries. However, the high sensitivity of specific capacity upon current rate indicates that the intrinsic kinetic property of $Mg_{1.03}Mn_{0.97}SiO_4$ must be poor, which should be further improved.

It is noted that two discharge voltage plateaus exist for all the as-prepared samples. For $Mg_{1.03}Mn_{0.97}SiO_4$, $Mg_{1.03}Mn_{0.97}SiO_4$/AB, and $Mg_{1.03}Mn_{0.97}SiO_4$/C, the corresponding discharge voltage plateaus are at 1.4/1.0, 1.5/1.1 and 1.6/1.2 V *vs*. Mg/Mg^{2+}, respectively. Carbon coating improves the interfacial conductivity and suppresses the voltage polarization, leading to the plateau enhancement. The two voltage plateaus may be explained by two kinds of energy sites with different geometrical and electrostatic limitations for the inserted Mg atoms in the magnesium deficient cathode material. This result is consistent with the crystal structure, as shown in Fig. 2.

Cyclic voltammograms using $Mg_{1.03}Mn_{0.97}SiO_4$ and $Mg_{1.03}Mn_{0.97}SiO_4$/C as the magnesium intercalation electrodes are shown in Fig. 6. There are two pairs of redox peaks marked as a, a′ and b, b′, respectively, which can be attributed to the intercalation and de-intercalation reactions. That is to say, the Mg^{2+} intercalation into the magnesium deficient positive electrode proceeds via two stages, which is in good agreement with the analysis of its crystal structure. Compared to $Mg_{1.03}Mn_{0.97}SiO_4$, the peak current density is much larger for $Mg_{1.03}Mn_{0.97}SiO_4$/C, and its oxidation peaks shift to the negative direction and the reduction peaks to the positive direction, indicating a decrease of the potential polarization. This result is in accordance with the discharging behavior observed on the Land battery measurement system.

The Nyquist plots obtained before charge and discharge are compared in Fig. 7 for the $Mg_{1.03}Mn_{0.97}SiO_4$ (a) and $Mg_{1.03}Mn_{0.97}SiO_4$/C (b) electrodes. The impedance diagram has three parts for both the samples. The high frequency small semicircle is due to the magnesium-ion transfer reaction in the surface film of the electrode, the low-middle frequency arc is due to the charge transfer reaction at the surface film/active material interface, while the inclined straight line in the low-frequency region rep-

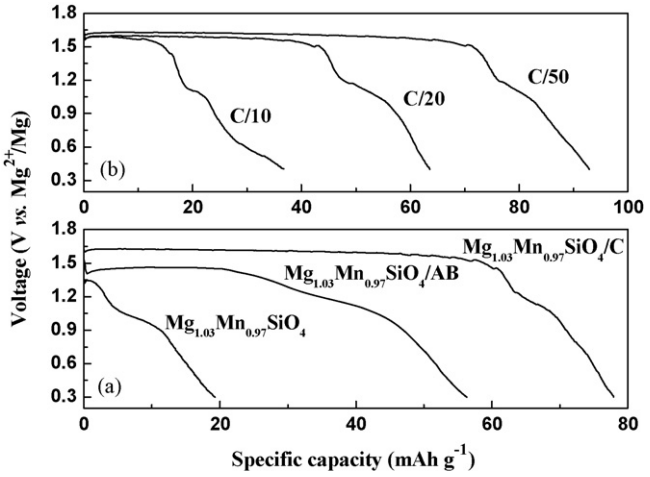

Fig. 5. Magnesium intercalation curves at a C/25 rate for $Mg_{1.03}Mn_{0.97}SiO_4$, $Mg_{1.03}Mn_{0.97}SiO_4$/AB, $Mg_{1.03}Mn_{0.97}SiO_4$/C (a), and for $Mg_{1.03}Mn_{0.97}SiO_4$/C at various rates (b), respectively.

Table 2
Equivalent circuit data of $Mg_{1.03}Mn_{0.97}SiO_4$ and $Mg_{1.03}Mn_{0.97}SiO_4/C$

Sample	R_e (Ω)	*CPE*1 C_f (μF)	R_f (Ω)	CPE2		R_{ct} (Ω)	CPE3 (μS)
				C_{dl} (μS)	n		
$Mg_{1.03}Mn_{0.97}SiO_4$	121.1	137	1.649×10^4	15.9	0.7888	577	153
$Mg_{1.03}Mn_{0.97}SiO_4/C$	78.86	1.954	1.173×10^4	8.954	0.8034	8.404	108.7

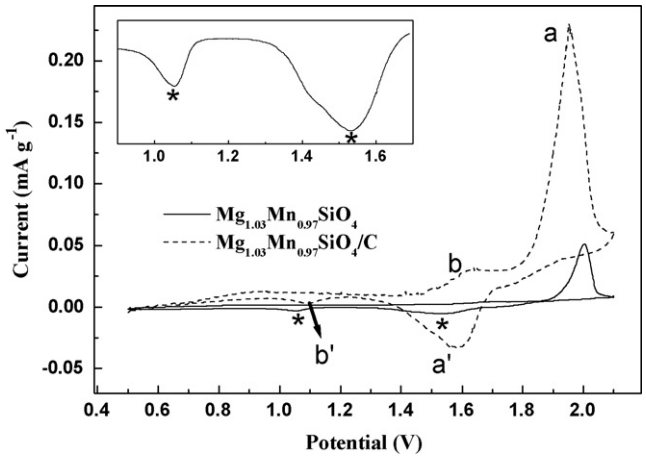

Fig. 6. Cyclic voltammograms of $Mg_{1.03}Mn_{0.97}SiO_4$ and $Mg_{1.03}Mn_{0.97}SiO_4/C$ measured at a scan rate of 5 mV s^{-1}. Insert is the segmental enlarged image using $Mg_{1.03}Mn_{0.97}SiO_4$ electrode.

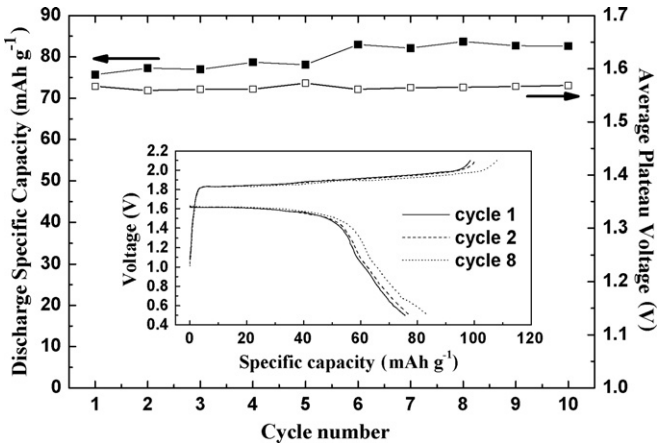

Fig. 8. Plots of discharge capacity *vs.* cycle number together with average plateau voltage *vs.* cycle number using $Mg_{1.03}Mn_{0.97}SiO_4/C$ electrode at a rate of C/25. Insert is the voltage-discharge specific capacity profile for the first, second and tenth cycles.

resents a diffusion-controlled process [22]. We find the diameter of the low-middle semicircle is reduced considerably for the $Mg_{1.03}Mn_{0.97}SiO_4/C$ electrode material. It means that the charge transfer resistance can be suppressed by a thin layer of carbon coating, which is an important reason for the lower voltage polarization and higher discharge capacity compared to the pure $Mg_{1.03}Mn_{0.97}SiO_4$. Relevant equivalent circuit is also shown in Fig. 7. The resistance contribution from the electrolyte and electrode is represented by R_e. Other parameters include: R_f and C_f related to surface film, R_{ct} and C_{d1} to charge transfer, and Warburg impedance Z_w. The parameters' values for said circuit elements of the two samples are shown in Table 2. Carbon coating results in a decrease of R_e, R_f and R_{ct} values. The improved electrode and interface behavior is consistent with the results of cyclic voltammetry tests and charge–discharge measurements.

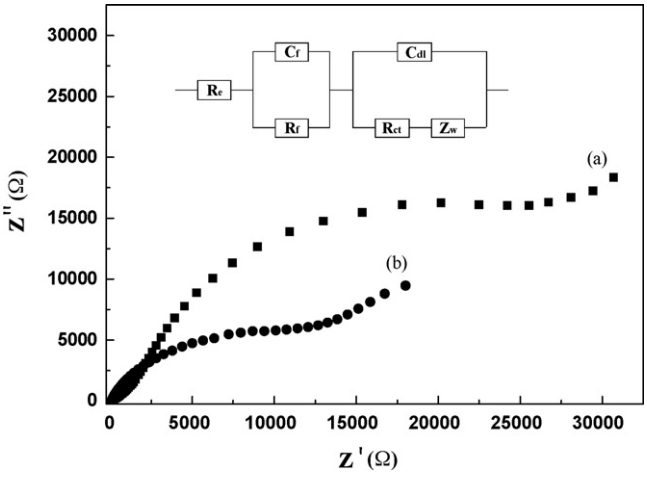

Fig. 7. Impedance plots for electrodes of $Mg_{1.03}Mn_{0.97}SiO_4$ (a) and $Mg_{1.03}Mn_{0.97}SiO_4/C$ (b). Insert is the equivalent circuit fitting the experimental data.

The magnesium intercalation/de-intercalation cycle behavior of $Mg_{1.03}Mn_{0.97}SiO_4/C$ material was also characterized. Plots of discharge specific capacity *vs.* cycle number together with average plateau voltage *vs.* cycle number using $Mg_{1.03}Mn_{0.97}SiO_4/C$ electrode at a rate of C/25 were shown in Fig. 8. A reversible intercalation/de-intercalation phenomenon could be observed, although the capacity of *ca.* 80 mAh g^{-1} is not high. Insert is the voltage-discharge specific capacity profile for the first, second and eighth cycles. It is noted that there is a capacity loss of *ca.* 20% during the first cycle. The structure defects of the electrode and the active phase as well as the slow magnesium-ion diffusion in the original silicate may be responsible for the initial irreversibility [23]. In addition, the initial electrochemical reaction may accompany with the electrolyte decomposition and surface filming on the electrode as often occurred on electrodes of lithium ion cells. This could also cause some electrochemical irreversibility. On the other hand, the voltage difference between intercalation and de-intercalation reduces and the discharge specific capacity becomes larger with the progressive cycle number. A reasonable explanation for this result is that the electrochemical activity of the $Mg_{1.03}Mn_{0.97}SiO_4/C$ is gradually activated during cycling. Owing to the low magnesium diffusion rate, it is difficult for the ions to transport within an $Mg_{1.03}Mn_{0.97}SiO_4$ particle and for charge transfer to occur on the surface. Therefore, diffusion tunnels have to be gradually established for the magnesium ions from the exterior to the interior of the particles. Only after such a procedure is completed, the voltage polarization can be suppressed to a certain degree and Mg-storage capacity reaches its maximum. More experimental and/or computational work will be needed to understand the detailed magnesium intercalation/de-intercalation mechanism and to improve the electrochemical performance.

4. Summary

Magnesium manganese silicates prepared by a sol–gel process exhibit distinct and reversible electrochemical intercalation

behavior. The nanosized powder configuration shortens ionic diffusion length within the particles and increases the contacting area between reactant phase and electrolyte. As a result, the electrochemical polarization is suppressed and the utilization of the active material is enhanced. Moreover, it is found that in situ carbon coating is an important step for improving the electrochemical performance. The intercalation voltage plateau for $Mg_{1.03}Mn_{0.97}SiO_4/C$ is as high as about 1.6 V *vs*. Mg/Mg^{2+}, and the specific capacity can reach to 92.9 mAh g^{-1} cycled at a C/50 rate. In light of its low cost and environment friendliness, magnesium manganese silicate could be a promising intercalation electrode material for advanced rechargeable magnesium batteries. An optimization of both the material structure and the electrolyte compatibility is necessary to increase the specific capacity and cycle performance.

Acknowledgements

This work was supported by National Natural Science Foundation of China (20603022) and National 973 Program (2007CB209700).

References

[1] P. Novák, W. Scheifele, O. Haas, J. Power Sources 54 (1995) 479.
[2] D. Aurbach, Z. Lu, A. Schechter, Y. Gofer, H. Gizbar, R. Turgeman, Y. Cohen, M. Moshkovich, E. Levi, Nature 407 (2000) 724.
[3] L. Sanchez, J.P.T. PereiraRamos, J. Mater. Chem. 7 (1997) 471.
[4] N. Kumagai, S. Komaba, H. Sakai, N. Kumagai, J. Power Sources 97 (8) (2001) 515.
[5] D. Imamura, M. Miyayama, Solid State Ionics 161 (2003) 173.
[6] H.T. Yuan, L.F. Jiao, J.S. Cao, X.S. Liu, M. Zhao, Y.M. Wang, J. Mater. Sci. Technol. 20 (2004) 41.
[7] L.F. Jiao, H.T. Yuan, Y.C. Si, Y.J. Wang, Y.M. Wang, Electrochem. Commun. 8 (2006) 1041.
[8] M.E. Arroyo-de Dompablo, M. Armand, J.M. Tarascon, U. Amador, Electrochem. Commun. 8 (2006) 1292.
[9] A. Nyten, A. Abouimrane, M. Armand, T. Gustafsson, J.O. Thomas, Electrochem. Commun. 7 (2005) 156.
[10] A.S. Prakash, P. Rozier, L. Dupont, H. Vezin, F. Sauvage, J.M. Tarascon, Chem. Mater. 18 (2006) 407.
[11] A. Nyten, S. Kamali, L. Haggstrom, T. Gustafsson, J.O. Thomas, J. Mater. Chem. 16 (2006) 2266.
[12] R. Dominko, M. Bele, M. Gaberscek, A. Meden, M. Remskar, J. Jamnik, Electrochem. Commun. 8 (2006) 217.
[13] Z.L. Gong, Y.X. Li, Y. Yang, Electrochem. Solid State Lett. 9 (2006) A542.
[14] Y.X. Li, Z.L. Gong, Y. Yang, J. Power Sources 174 (2007) 528.
[15] R. Dominko, M. Bele, A. Kokalj, M. Gaberscek, J. Jamnik, J. Power Sources 174 (2007) 457.
[16] A. Kokalj, R. Dominko, G. Mali, A. Meden, M. Gaberscek, J. Jamnik, Chem. Mater. 19 (2007) 3633.
[17] V.V. Politaev, A.A. Petrenko, V.B. Nalbandyan, B.S. Medvedev, E.S. Shvetsova, J. Solid State Chem. 180 (2007) 1045.
[18] F. Zhou, M. Cococcioni, K. Kang, G. Ceder, Electrochem. Commun. 6 (2004) 1144.
[19] Y.Q. Wang, J.L. Wang, J. Yang, Y.N. Nuli, Adv. Funct. Mater. 16 (2006) 2135.
[20] S.Y. Chung, J.T. Bloking, Y.M. Chiang, Nat. Mater. 1 (2002) 123.
[21] W. Xing, J.S. Xue, J.R. Dahn, J. Electrochem. Soc. 143 (1996) 3046.
[22] J. Fan, P.S. Fedkiw, J. Power Sources 72 (1998) 165.
[23] A.S. Andersson, J.O. Thomas, J. Power Sources 97/98 (2001) 498.